Maximum Rate of Crystallization and Morphology of Random Propylene Ethylene Copolymers as a Function of Comonomer Content up to 21 mol %

K. Jeon, Y. L. Chiari, and R. G. Alamo*

Department of Chemical and Biomedical Engineering, College of Engineering, Florida Agricultural and Mechanical University and Florida State University, 2525 Pottsdamer Street, Tallahassee, Florida 32310-6046

Received March 29, 2007; Revised Manuscript Received October 10, 2007

ABSTRACT: We report a study of the primary chain microstructure, crystallization kinetics, and crystalline morphologies of propylene ethylene copolymers (PE) synthesized with metallocene catalysts in a range of ethylene up to 21 mol %. A ^{13}C NMR triad distribution analysis lends support for a random distribution of the comonomer in the complete series. Melting (T_m) and crystallization (T_c) temperatures decrease with increasing ethylene more rapidly than the decrease of the glass transition temperature (T_g). Consequently, for ethylene >10 mol % the crystallization is observed at T_cs relatively close to T_g allowing to observe experimentally the maximum of the crystallization rate. In the low T_c range, segmental dynamics play a prominent role in developing the semicrystalline structure, and the crystallization rate decreases dramatically with increasing molar mass. For a fixed molar mass and undercooling, the strong decrease of the crystallization rate with increasing ethylene, especially for copolymers with >10 mol %, correlates with analogous depletion of crystallizable sequences. A similar trend is predicted for the stereo defect. Analysis of the temperature dependence of the rates following nucleation and growth theory led to values of T_m^o comparable to those obtained from equilibrium relations. PEs develop γ phase in the complete range of ethylene studied. However, the γ phase is not found at $T_c < T_{max}$ (rate maximum), indicating that in addition to short crystallizable sequences, considerable molecular diffusion is required to form this polymorph. As T_c approaches T_g, the effects of nucleation and segmental transport on crystallization affect the lamellar morphologies. Numerous short rodlike lamellae are formed at T_c close to T_g, while sheaflike lamellar structures similar to those found in propylene 1-hexenes (PH) of matched comonomer content (>10 mol %) develop at the highest T_cs, yet in PEs a different crystalline unit cell is not found. The ability to propagate long crystalline lamellae by PEs and PHs copolymers as a consequence of the accommodation of a high content of comonomer in the crystalline lattice is discussed.

Introduction

Random copolymers of propylene and ethylene produced with a metallocene catalyst have advantages over similar types of copolymers made with classical Ziegler−Natta catalysts. In the metallocene type, molar mass distribution and interchain distribution of the comonomer are narrow, and the intrachain comonomer distribution follows Bernoullian statistics. Conversely, classical Ziegler−Natta catalysts lead to broadly distributed copolymers in both molar mass and comonomer concentration complicating the study of structure−properties relations.

With propylene copolymers synthesized with metallocene catalysts it is possible to investigate the influence of type and concentration of defects (comonomer and stereo and regio types) on the thermodynamic behavior, the kinetics of phase transformation and the formation of the γ polymorph, a crystallographic phase with nonparallel molecules unprecedented in the scope of crystalline polymers. Earlier works of the crystallization properties of metallocene iPP copolymers covered a relatively narrow range of comonomer (<10 mo%).[1−3] With recent developments in metallocene catalysts, it is now possible to synthesize random copolymers in a much broad range of comonomer contents. Packing characteristics specific of a given comonomer type were revealed by studying 1-alkene iPP-based copolymers in a range of comonomer >10 mol %. This was not predicted from the studies in the low comonomer range.[4−7] Examples are copolymers with 1-hexene and 1-butene units. Metallocene 1-hexene and 1-butene iPP copolymers with <10 mol % comonomer are di-isomorphic, they pack in a mixture of α (monoclinic) and γ (orthorhombic) phases, while at comonomer contents >15 mol %, the 1-hexene units, not incorporated in the crystals at low levels, cocrystallize with the propene units in a trigonal more dense packing.[5,6] Contrasting with this behavior, the 1-butene units are easily incorporated in the crystals at all comonomer levels causing expansion of the lattice. At contents >18 mol % the expansion of the *a*-axis of the α lattice from the butene incorporation is too large to allow the homoepitaxial growth of the γ polymorph. For this and higher comonomer levels, γ no longer develops in PB copolymers.[7] Polymorphism in propylene ethylene copolymers has been studied as well but only up to 13 mol % ethylene in the most recent work.[1,7] Therefore, any influence of the ethylene counit at levels >13 mol % on the di-isomorphic (α and γ) structure of these copolymers is yet unknown. This work addresses the role of crystallizable sequence length on the crystallization kinetics and polymorphism at sub and upper ambient temperatures, primarily in a range of ethylene >10 mol %. The significance of increasing ethylene on the mechanical behavior of these copolymers is a change of properties from thermoplastic at the relatively low content to elastomeric behavior for ethylene contents above 15 mol %.[8] Correspondingly, the range of applications changes broadly, making more relevant to correlate the type and evolution of the crystalline

* Corresponding author. E-mail: alamo@eng.fsu.edu.

10.1021/ma070757b CCC: $40.75
Published on Web 12/11/2007

structure with the primary molecular structure of these copolymers.

Previous analyses by ^{13}C NMR spectroscopy demonstrated the inclusion of the ethylene unit in the crystalline lattice at levels that scale proportionally to the concentration of ethylene in the chain.[9] Moreover, the ethylene unit acts as a defect that is accumulated at a higher concentration in the amorphous regions than in the crystalline ones.[9] Hence, with increasing ethylene in the chain, a large decrease in crystallinity is observed due to the overall reduction in crystallizable sequence lengths. Melting and crystallization temperatures also decrease quickly with increasing ethylene in light of the increased composition in the melt of the less crystallizable ethylene counits.[8,9] Two previous works of iPP copolymers with 1-hexene and 1-octene as comonomers have shown that in reference to the homopolymer, while the melting and crystallization temperature decreases very rapidly with increasing comonomer content, the decrease in the glass transition temperature in the same range of comonomer is significantly shallower.[4,10] Effectively, with increasing comonomer the crystallization of elastomeric propylene copolymers occurs at temperatures that approach the glass transition. As a consequence, while the energy barrier of the crystallization is dominated by the nucleation term in the observable crystallization temperature range of iPP and low ethylene copolymers, both nucleation and diffusion driven energy barriers are predicted to be operative and to compete in the crystallization of iPP copolymers with high comonomer contents and to be driven by the transport term at temperatures close to T_g.

A major focus of this work is to document that the increase of comonomer extends the range of crystallization kinetics to undercoolings where the free energy change for segmental transport dominates over the nucleation term and brings the opportunity to analyze the crystallization kinetics and associated lamellar morphologies of polyolefins above and below the maximun of crystallization rates. To be best of our knowledge, the experimental observation of maxima of the crystallization rates with temperature, as shown in this work, has not been reported for random isotactic propylene-based 1-alkene copolymers.

A second objective is to address the effect of the ethylene on the crystallization rates in reference to the effect on the rates given by the stereo (*mrrm*) defect. All experimental evidence indicates a basically equivalent partitioning of the ethylene and the stereo defect between crystalline and noncrystalline regions and the same effect on the polymorphic behavior of metallocene iPPs.[7] Given that for the stereo and ethylene defects the formation of the γ phase and the crystallization rates are governed by the length of crystallizable sequences, the variation of the crystallization rates with increasing ethylene are predicted to follow the same behavior as for iPPs with increasing contents of *mrrm* defects. Any rate comparison at a fixed undercooling requires knowledge of the equilibrium melting temperature T_m^o, and based on values of this parameter obtained by the Hoffman−Weeks (H−W) extrapolation, it was concluded in an earlier work that the stereo defect increases the crystallization rate.[11] However, as described by Crist[12] the applicability of this extrapolation is questionable because the stereo and the ethylene defects are partially rejected from the crystals.[9,13] In view of the limited applicability of the H−W extrapolation, in the present work, the variation of the rates with increasing ethylene at a constant undercooling is analyzed in reference to T_m^o data obtained from equilibrium relations. This is possible because the concentration of ethylene inside the crystal is known from NMR. Values of T_m^o of the copolymers (>10 mol % ethylene) are also estimated, and compared to theoretical values, from best fits of the experimental rate data with nucleation and growth models.

Table 1. Molecular Characterization of Metallocene Propylene Ethylene Copolymers

sample	ethylene (mol %)	stereo (mol %)	regio (mol %)	total defects (mol %)	$M_w \times 10^{-3}$ (g/mol)	M_w/M_n
PE1.8	0.8	0.6	0.4	1.8	233	1.98
PE2.8	1.7	0.7	0.4	2.8	221	1.81
PE3.4	2.2	0.7	0.5	3.4	215	1.75
PE5.8	4.6	0.8	0.4	5.8	251	2.12
PE8.7	7.5	0.8	0.4	8.7	188	1.71
PE10.1	7.5	1.7	0.9	10.1	188	2.36
PE16.9	14.7	1.3	0.9	16.9	196	∼1.80
PE20.8	18.5	1.3	1.0	20.8	134	∼1.80
PE22.5	20.8	0.8	1.0	22.5	235	∼1.80

Experimental Section

The propylene ethylene (PE) copolymers studied are experimental samples obtained with bridged Exxpol metallocene catalyst.[14,15] Their molecular characterization is given in Table 1. The sample designation encodes the type of comonomer and the total defect content. The type and fractional content of all the defects was obtained from solution-state ^{13}C NMR spectra where assignments of ethylene containing sequences were made according to published literature data.[16−19] The ethylene content was calculated adding the fractional content of all E centered triads.[16] The content of stereo defects was obtained from the *mrrm* pentad at 19.5 ppm.[20] Propylene 2,1 additions of the erythro and threo types were found in all copolymers, and quantified from the resonances in the 34.6−34 ppm region.[21,22] Defects of the 1,3 type were not observed. The analysis of experimental data throughout the text is referred to the total concentration of all types of defects, also listed in Table 1. The molar mass and its distribution was determined by standard gel permeation chromatography. Note that except for one copolymer of the series, the molar mass is essentially constant at ∼200 000 g/mol.

^{13}C NMR spectra were obtained in a Bruker AC-300 NMR spectrometer with a ^{13}C resonance frequency of 75.468 MHz using ∼6.5 w/v % homogeneous solutions of the copolymers in 1,1,2,2-tetrachloroethane-d_2 in 10 mm o.d. NMR tubes. The spectra were recorded at 80 °C (for 15 mol % ethylene and higher) or 125 °C (ethylene content lower than 15 mol %), respectively. The data were acquired using acquisition times of 1.36 s, relaxation delay of 10 s, a 15 ms pulse corresponding to a 45° angle, a spectral width of 6024 Hz, and 6724 to 21700 transients per data file.

The original powder or pellets were sandwiched between thin Teflon films and compression molded in a Carver press at 180 °C to films ∼0.6 mm thick. After melting for ∼5 min in press, the films were taken at room temperature and left for 2 weeks prior to initial DSC melting. Given that the two copolymers with the highest ethylene content display rather slow crystallization kinetics at room temperature, this aging step is important to compare thermal properties among the series at a stage when most of the crystalline structure has evolved. About 7 mg of these films were used for thermal analysis using a Perkin-Elmer differential scanning calorimeter DSC-7 under nitrogen flow. Temperature and heat flow calibrations were carried out with indium as standard. The first heating thermogram, the cooling thermogram, and the second heating thermogram were recorded at 10 °C/min.

Isothermal crystallizations were carried out either in the DSC or in controlled temperature baths. Overall crystallization rates were obtained from the DSC exothermic peaks as the inverse of the time required for 50% of the transformation to take place (equivalent to the half time rate concept).[23] The degree of transformation, at a fixed isothermal temperature, was followed by the variation of the heat-flow vs time in the DSC-7. To maximize heat transfer, the DSC was operated in conjunction with an intracooler and under

dry nitrogen flow. For copolymers that develop very low degrees of crystallinity (PE 22.5), the exothermic peak could not be resolved. Here the extent of the transformation was obtained from the endotherm by measuring the degree of crystallinity with time. Some kinetic data at crystallization temperatures with very long time scales required carrying out crystallizations outside the DSC. In these cases, the copolymers were crystallized in thermostated constant temperature baths with accuracy better than ±0.1 °C. Sealed DSC sample pans were inserted into glass test tubes, and melted in a laboratory oven at 180 °C for approximately 10 min. The test tubes were then quickly transferred from the oven to heated or refrigerated baths, previously set at a fixed crystallization temperature. After a desired crystallization time had elapsed, the samples were placed in the DSC cell and melted at 10 °C/min.

Isothermally crystallized specimens at above and subambient temperatures for wide-angle X-ray scattering (WAXS) analyses were prepared carrying out similar crystallization procedures in the baths. The original pellets were weighed to fill an aluminum square mold of approximately 10 mm long, 10 mm wide, and 0.8 mm thick, and molded using the Carver press. The sandwich was placed in a glass tube evacuated and sealed under vacuum. Following crystallization, the tubes were quenched in tap water, and the samples removed when the temperature reached ambient conditions. The melting thermogram of the isothermally crystallized copolymers was recorded for adherence to the values obtained after crystallization in the DSC.

Ambient temperature WAXS diffractograms were taken in a slit collimated Siemens D500 diffractometer in a 2θ range of 5−40°. Subambient WAXS diffractograms were obtained using a commercial Peltier device. Diffractograms above room temperature were collected in a Siemens D500 $\theta-\theta$ diffractometer with an attached Anton Paar HTK high-temperature head. The diffractometers were calibrated with powered corundum (α-Al_2O_3). Filtered Cu Kα radiation was used as a source, and both diffractometers were operated at 30 mA and 40 kV. Peak assignments for the α and γ phases followed those given by Brückner and Meille[24] and Turner-Jones.[25] The fraction of the γ polymorph was calculated from the areas of the (117) γ reflection at $2\theta = 20.1$ and the (130) α reflection at $2\theta = 18.8$, as $A_\gamma/(A_\gamma + A_\alpha)$, after subtraction of the amorphous halo. Extraction of peak areas from crystalline diffraction patterns was done using GRAMS.[26] Quantifying the fraction of γ phase from diffractograms with weak reflections, such as those for PEs > 10 mol % is subject to large discrepancies depending on the method used to obtain the intensities of the α and γ crystal peaks. In this study we encountered that the diffractogram of a model atactic polypropylene used previously to subtract the halo of diffractograms of low ethylene copolymers[1] did not match the amorphous pattern of PEs >10 mol % ethylene. We believe the reason is the significant change in free volume in the melt with increasing ethylene and the corresponding impact in density of the amorphous regions.[27] In order to properly scale and subtract the diffractogram of the amorphous regions, diffractograms of PEs with ethylene >10 mol % were obtained at different temperatures in the melt. The linear thermal expansion of the halo ($2\theta_{halo} = -0.008T + 17.4$) was used to shift the diffractogram of the melt to the corresponding value for T_c > 25 °C. The procedure and the determination of the content of γ phase using mixed Gaussian + Lorentzian peaks to fit the resulting crystalline pattern is given as Supporting Information.

Specimens for atomic force microscopy (AFM) were prepared by melting approximately ~1 mg of sample between two coverslips and rapidly submerging the sandwich into liquid Nitrogen. One coverslip is easily removed with this method. The film (~50 μm thick), with one free surface, was placed on a Linkam hot stage, heated to 180 °C for 3 min, and crystallized isothermally by rapid cooling from the melt to T_c. AFM images were recorded in an environmental JEOL 4210 scanning probe microscope using Olympus single side coated silicon cantilevers (spring constants of ~ 40 N/m and a tip radius of less than 10 nm) at a resonant frequency of ~300 kHz. Topographic and phase images were simultaneously collected under ambient conditions in noncontact AC mode at 256 × 256 standard resolution. Lamellar thicknesses were measured from 0.6 × 0.6 μm phase images using the JEOL software. See Supporting Information.

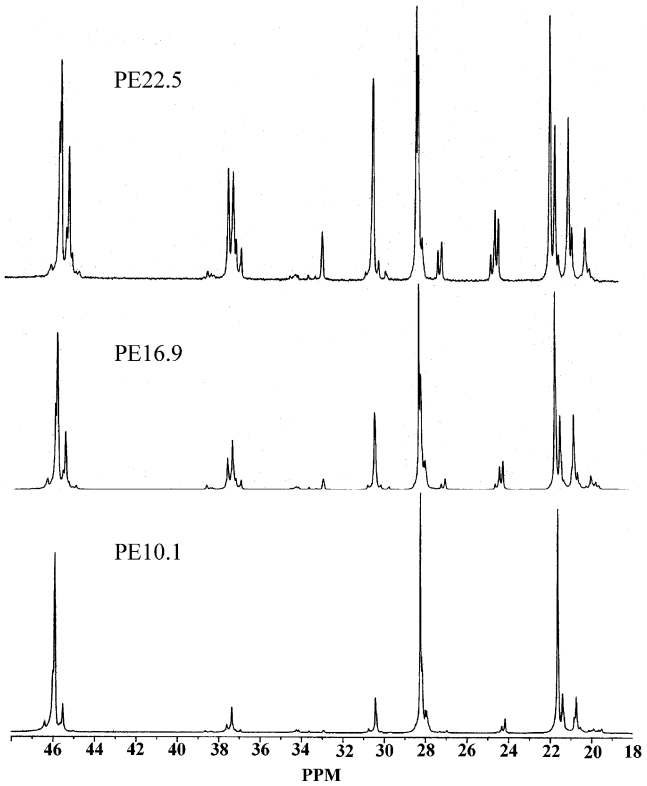

Figure 1. ^{13}C NMR spectra of selected metallocene propylene ethylene copolymers. Sample designation follows Table 1.

Results and Discussion

Primary Molecular Structure. Melting and crystallization of propylene and ethylene copolymers are known to be very sensitive to the comonomer distribution.[28−30] The samples investigated were copolymerized using a "single site" metallocene catalyst, known to produce copolymers with a narrow interchain comonomer distribution. In addition, the intrachain distribution of the ethylene is expected to be random.[31] In the course of the investigation of the crystallization kinetics of these copolymers we encountered that PE20.8 and PE22.5 present very large differences in kinetics, larger than expected from the difference in total defects. It was, hence, important to rule out that this difference was due to a blocky comonomer distribution in the higher crystallizing copolymer.

A test of the random distribution within the series of copolymers listed in Table 1 was carried out analyzing the experimental ^{13}C NMR spectra. The spectra of three representative copolymers are given in Figure 1. The collective assignments method described by Randall was used to carry out a triad distribution analysis from the observed resonances.[16] From the spectra, the experimental values of all possible triads are compared with calculated values according to Bernoullian and first-order Markovian models in Figure 2. The Bernoullian describes the random distribution because the probability of a monomer addition is independent of the outcome of a previous addition, while in Markov models the addition of a monomeric unit depends on preceding events. Experimental sequences that deviate strongly from the models expectation, especially those that correspond to consecutive ethylene units, are a signature of blocky distributions.

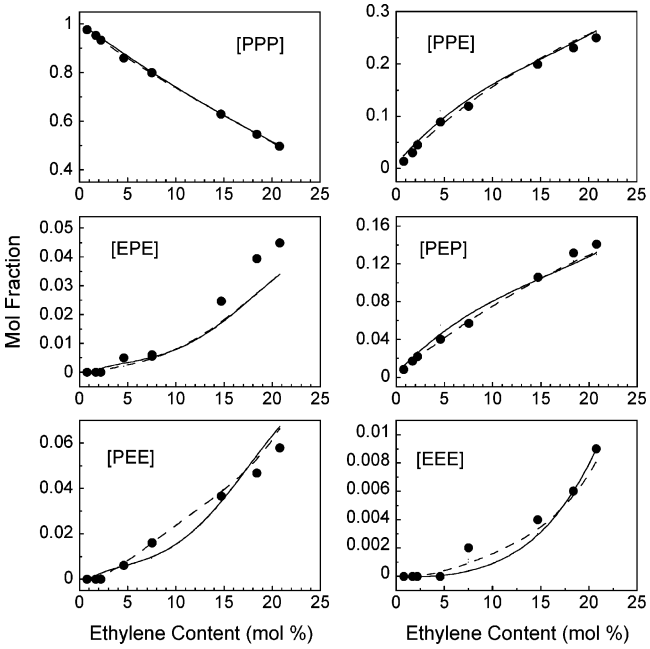

Figure 2. Observed and calculated compositional triad sequence distribution for metallocene propylene ethylene copolymers. Key: continuous line, theoretical Bernoullian prediction; dashed line, theoretical Markovian prediction.

Figure 2 reveals that except for the EPE triad that presents some deviations at the higher comonomer level, both models provide adequate fits for the observed triad distributions.[16,18] At a high confidence level both models predict triads PPP, PPE, and PEP and give good adherence to the observed values for the E centered triads. The NMR intensity of usually weak EEE signals is better resolved for copolymers with high ethylene concentration, such as those pertaining to copolymers PE20.8 and PE22.5; for these copolymers the fit follows closely the Bernoullian distribution. This gives us confidence that the distribution of ethylene in these copolymers follows a random pattern.

The observed product of reactivity ratios $r_p r_e$, and the number-average sequence length (n_p) were also compared with predictions for Bernoullian and first-order Markovian distributions. $r_p r_e$ values were calculated following well-known relations from the experimental dyas or triads according to[32,33]

$$r_p r_e = \mathrm{EE[PP/(PE/2)]^2} \tag{1}$$

$$r_p r_e = 1 + \left(\frac{\mathrm{P}}{\mathrm{E}}\right)\left(\frac{\mathrm{EEE} + \mathrm{PEE}}{\mathrm{PEP}} + 1\right) - \left(\frac{\mathrm{P}}{\mathrm{E}} + 1\right)\left(\frac{\mathrm{EEE} + \mathrm{PEE}}{\mathrm{PEP}} + 1\right)^{0.5} \tag{2}$$

The reactivity ratio product for a Bernoullian system is 1.0, and for a first-order Markovian analysis is given by[34]

$$r_p r_e = \frac{P_{pp}(1 - P_{ep})}{P_{ep}(1 - P_{pp})} \tag{3}$$

where P_{pp} and P_{ep} are the conditional probabilities for the propagation of propylene and ethylene units respectively.

The products of reactivity ratios $r_p r_e$ calculated from the observed distributions according to eq 1 are compared with the calculated values in Table 2. Equation 2 leads to very similar data for $r_p r_e$. The observed values, in a range of 0.8−2.0, are much lower than those commonly reported for copolymers obtained with a Ziegler−Natta catalyst,[32,35,36,37] and hence are also indicative of a random distribution. A simple comparison of the $r_p r_e$ values indicates that the distribution of all the copolymers of the series follows a first-order Markovian model more closely than the Bernoullian model. Other indicators, such as the number-average sequence length, $\bar{n}_P$, also listed, are less sensitive to the small differences between the Bernoullian and Markov propagation at the investigated triad level. In relevance to studies of the effect of increasing comonomer in the crystallization kinetics, lack of significant deviations in the values of a specific triad in Figure 2 for any of the copolymers studied, respect to the behavior of the other samples, supports the same ethylene distribution among the series. More specifically the ethylene distribution of PE20.8 and PE22.5 follows the same pattern, and differences in crystallization kinetics between these copolymers must be found outside a deviation from the essentially random pattern.

Thermal Transitions. The final observable melting temperatures (T_{m_f}) of rapidly crystallized copolymers kept for ∼2 weeks at room temperature, the peak crystallization temperatures (T_c), and the glass transition temperatures measured by DSC (T_g) are plotted against the total concentration of defects in Figure 3. The observed melting point−composition behavior is the expected for random copolymers and correlates with a decreasing crystalline sequence propagation probability as the content of ethylene in the copolymer chain increases. Overall, these thermal data serve as reference of the temperature interval where crystallization kinetics can be experimentally followed in this series. Melting and crystallization temperatures decrease with ethylene content at much faster rates than the variation of T_g.[38,39] The line that joins experimental crystallization peaks joins the T_g line at a defect content ∼20 mol %, explaining the lack of a crystallization exotherm for copolymers with a content of ethylene above 15 mol %. Accordingly, the crystallization of copolymers with high ethylene contents could only take place in a narrow temperature interval and at temperatures close to their T_g. The enthalpy of fusion decreases linearly from 90 to 7 J/g with increasing defects and points to a rapid decrease in crystallinity with increasing ethylene (also observed by WAXS). The decrease in crystallinity accounts for the restrictions posed by the comonomer to the development of the crystalline structure in spite of the partial inclusion of the ethylene units in the crystalline regions.[9]

Crystallization Kinetics. Isothermal crystallization exotherms are given in Figure 4 for PE10.1 (a), PE16.9 (b), and PE20.8 (c) for increasing crystallization temperatures (T_c). The exotherms for copolymers with lower ethylene content (not shown) display similar trends to those of PE10.1. As expected from the variation between T_c and T_g in Figure 3, the T_cs at which isothermal crystallization can be followed decrease dramatically with increasing ethylene and other irregularities in the propylene chain. The temperature interval shifts from 112 to 120 °C for PE1.8 to a broad range from −15 to +40 °C for PE16.9. Most significant is the variation of the time required to reach the exothermic peak maximum ($t_{1/2}$). This time increases systematically with increasing T_c in copolymers with ethylene content up to ∼10 mol % (Figure 4a). Copolymers with ethylene above ∼10 mol % have $t_{1/2}$ values that first decrease with decreasing T_c, reach a minimum value, and then increase again with further decrease of T_c. This change is illustrated in Figure 4, parts b and c, for PE16.9 and PE20.8, respectively. Identifying the inverse of this value with the overall crystallization rate, the data show that the maximum of the crystallization rate (T_{max}) is ∼40 °C above T_g, and located at a

Table 2. Observed vs Calculated Conditional Probabilities, P_P, P_{PP}, and P_{PE}; Product of Reactivity Ratio, $r_P r_E$; and Propylene Number Average Sequence Length, $\bar{n}_P$, Where Obs Are Observed Values and B and M Stand for Bernoullian and Markovian, Respectively

	conditional probabilities				$r_e r_p$			$\bar{n}_P$		
			M							
copolymer	Obs P	B P_P	P_{PP}	P_{EP}	Obs eq 1	B eq 1	M[a] eq 3	Obs[b]	B[c]	M[d]
PE5.8	0.954	0.938	0.951	0.925	1.20	1.00	1.59	20.47	16.03	20.58
PE8.7	0.925	0.912	0.933	0.877	1.90	1.00	1.95	14.11	11.44	14.89
PE10.1	0.925	0.929	0.930	0.875	2.02	1.00	1.91	14.21	14.14	14.30
PE16.9	0.853	0.858	0.858	0.847	1.05	1.00	1.10	6.86	7.04	7.07
PE20.8	0.816	0.819	0.817	0.820	0.82	1.00	0.98	5.27	5.51	5.47
PE22.5	0.792	0.794	0.792	0.800	0.81	1.00	0.95	4.67	4.85	4.80

[a] The P_{PP} and P_{EP} values were obtained from a linear regression fit of the experimental triad distributions. [b] For experimental data, $\bar{n}_P = [PP] + (1/2)([PE] + [EP])/(1/2)([PE] + [EP])$. [c] For a Bernoullian distribution, $\bar{n}_P = 1/1 - P_P$. [d] For a Markovian distribution, $\bar{n}_P = 1/P_{PE}$.

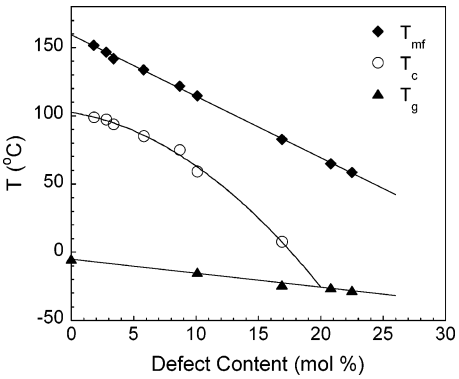

Figure 3. Final melting (T_{mf}), crystallization (T_c) and glass transition temperatures (T_g) as a function of total defects. Cooling and heating rates are 10 °C/min.

temperature between 10 and 20 °C for PE16.9 and between 5 and 10 °C for PE20.8

Any attempts to observe isothermal crystallization exotherms in the DSC from PE22.5 were unsuccessful; hence, the values of $t_{1/2}$ were obtained from the endotherms after halting isothermal crystallization for different times. The endotherm procedure was also followed for PE16.9 and PE20.8 at the highest and lowest T_cs. An example for $T_c = 25$ °C is given in Figure 5 to illustrate the impact of kinetics in developing the crystalline structure of copolymers with high ethylene content at ambient temperature. Here, the temporal development of crystallinity is compared for copolymers in a range of ethylene content between 7.5 and 21 mol %. The crystallization of PE10.1 is nonisothermal, and the data for PE16.9 derive from the exotherm. The initial rates decrease exponentially with the concentration of defects; thus, while PE16.9 requires less than 5 min to develop half of the crystallinity, it takes over 1300 min for PE22.5 to develop half of the transformation. As a consequence of their slow kinetics, PEs with >10 mol % ethylene require prolonged room temperature aging to fully develop their semicrystalline morphology.

The crystallization rate as $\ln(1/t_{1/2})$ is plotted as a function of T_c in Figure 6 for all PE copolymers in a compositional range from 0.8 to 21 mol % ethylene. The accessible T_c interval to observe crystallization kinetics shifts to lower values with increasing comonomer content reflecting the dependence of the rate with undercooling ($T_m^o - T_c$), and the decrease of T_m^o with increasing ethylene. A major feature in the overall crystallization rate plot of Figure 6 is that relatively large contents of randomly placed ethylene (>∼10 mol %) in the iPP chain lower the temperature interval for observing isothermal crystallization to a range that approaches the glass transition temperature. At these relatively low temperatures, the increased melt viscosity and a low concentration of crystallizable sequences, decrease crystallization rate to the point that crystallization kinetics could be followed in the diffusion driven range, to the left of the maximum, as well as in the nucleation controlled region, at T_c

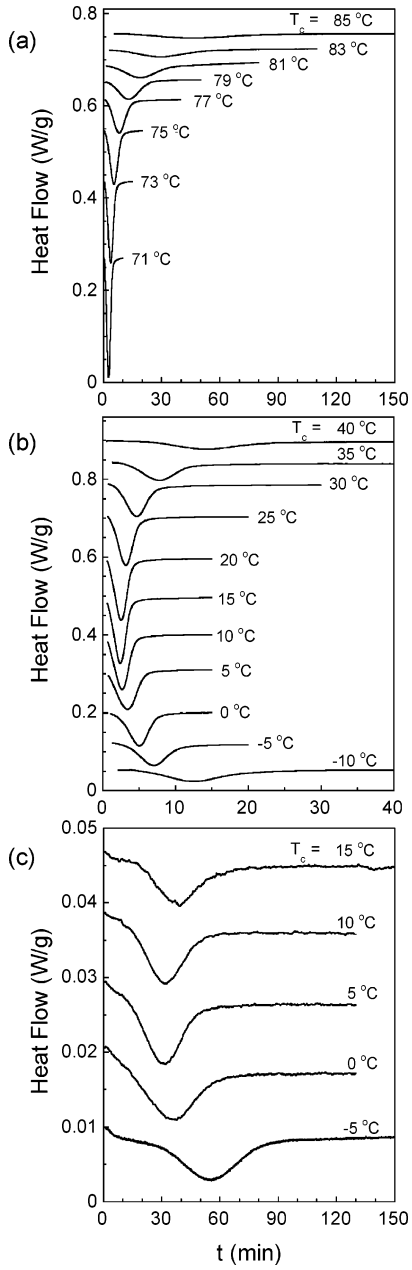

Figure 4. DSC isothermal crystallization thermograms of (a) PE10.1, (b) PE16.9, and (c) PE20.8 at the indicated crystallization temperatures. Thermograms are shifted in the *y* axis for clarity.

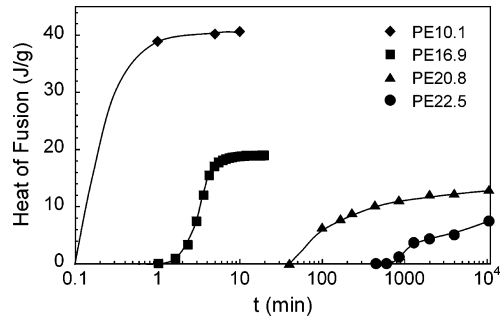

Figure 5. Evolution of enthalpy with time for PE copolymers crystallized at 25 °C.

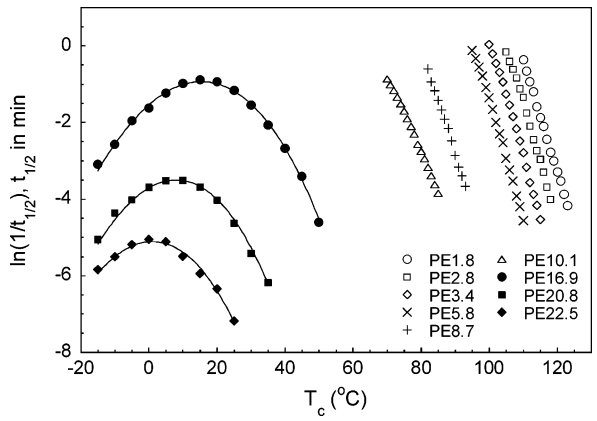

Figure 6. Overall crystallization rate expressed as $\ln(1/t_{1/2})$ as a function of crystallization temperature for all copolymers listed in Table 1. Solid lines for PE16.9, PE20.8, and PE22.5 are best fits for the formation of a 3D nucleus using a Vogel−Fulcher transport term.

$> T_{max}$. Remarkably, the crystallization kinetics of PE copolymers with ∼20 mol % defects could be followed at −15 °C, this is only ∼10 degrees above the T_g of these copolymers measured by DSC.

Copolymers with less than ∼10 mol % ethylene reach fast crystallizations at T_cs sufficiently far from T_g, hence, the rate maximum is not observed. The temperature at which the rate is a maximum is a function of the content of ethylene. It decreases from 17 °C for PE16.9 to 8 °C for PE20.8 and to 1 °C for PE22.5, respectively. Observation of the maximum crystallization rate is possible in these copolymers because the metallocene catalyst used led to a random distribution of the comonomer. Consequently, with decreasing ethylene, the distribution of isotactic sequence lengths is continuously displaced to longer runs. Overall, the ethylene units are defects that hinder crystallization, in spite of their partial inclusion in the lattice; therefore, it is expected that upon crystallization, segments containing the longest crystallizable sequences (led by the longest isotactic runs) are first selected. The number of such runs decreases with content of ethylene in the copolymer, and the crystallites formed from these sequences are only stable at much lower temperatures. Thus, the continuous variation of crystallizable sequence lengths among the copolymers, and kinetic stability of the crystallites, explain the lowering of the crystallization temperatures with increasing ethylene and the observation of the maximum rate. A maximum in the overall rates with T_c was also observed in a syndiotactic polypropylene (87.3 mol % rr) synthesized with a metallocene catalyst.[40] In contrast, copolymers synthesized with Ziegler−Natta catalysts have blocky-type comonomer distributions where long isotactic runs are found in copolymers with low and high comonomer contents.[23] The long isotactic runs of Z-N copolymers lead to relatively fast crystallizations, invariably far from T_g, and prevent observation of the crystallization rate maxima.

An additional feature of interest is the strong effect of molar mass on kinetics found when a comparison is made between $t_{1/2}$ of PE20.8 (110 min) and PE22.5 (1300 min) in Figures 5 and 6. These two copolymers differ only by 1.7 mol % ethylene and have similar contents of stereo and regio defects, therefore, their T_m^o value is not expected to differ greatly. Their major structural difference is their molar mass. PE20.8 has a molar mass of 134 000; this is about half the value of PE22.5 (235 000). The heat of fusion of the lower molar mass copolymer is nearly double and the crystallization kinetics ten times faster than for PE22.5. Since differences in their composition distribution were ruled out by the NMR triad analysis, we conclude that at a relatively high level of comonomer (∼20 mol %), the impact of molar mass, and hence entanglements, on the crystallization kinetics is more pronounced than for copolymers with a lower level of ethylene. For a more quantitative comparison we take, for example, the $t_{1/2}$ given by De Rosa et al. for iPP with $M_v = 68\,000$ and $M_v = 205\,000$ at the same ∼1 mol % defect content.[41] At a fixed undercooling, the iPP with the lower molar mass crystallizes at a faster rate but the difference in $t_{1/2}$ with the higher molar mass iPP is less than 5 min.[41] Hence, the differences in $t_{1/2}$ of >1000 min with molar mass observed between PE20.8 and PE22.5 in Figure 5 are not found in the homopolymer or in other lower comonomer content random copolymers.[42] In the latter the crystallization kinetics is observed in a temperature range far from T_g, with minor restrictions to segmental transport.[23] In propylene copolymers with ethylene >15 mol %, the crystallization is observed at temperatures approaching T_g, and hence from a more viscous melt. Here, a simple viscosity argument to diffuse the small concentration of crystallizable segments to the initial nucleus site leads to rates proportional to M^3 or a ratio of 5.4 between PE22.5 and PE20.8.[43] It turns that this ratio is within the range of rate ratios in the diffusion driven crystallization range of these copolymers. Thus, in addition to the 1.7 mol % difference in ethylene, the difference in rates between PE22.5 and PE20.8 support the notion that near T_g slower segmental dynamics have a greater impact in the segmental transport of the more entangled chains, thus resulting in significantly retarded crystallizations.

The combined effect of stereo and regio defects decreasing $t_{1/2}$, independently from the comonomer effect, is also evident in Figure 6 when the rate data for PE8.7 and PE10.1 are compared. These copolymers have the same ethylene content (7.5 mol %) but differ by a ratio of ∼2 in the content of stereo and regio defects. At a fixed T_c, PE10.1 with ∼1 mol % higher content of stereo and regio defects than PE8.7, displays a significantly higher $t_{1/2}$ (an apparent lower rate). Hence, the differences in kinetics of these two copolymers are due to errors in the propagation of the iPP units and point out the importance of accounting for the type and concentration of all defects, other than the comonomer units, when studying the crystalline properties of poly(propylene) and its copolymers.[44] De Rosa et al. have investigated extensively the effect of content and distribution of isolated inversions of the *mrrm* type on the crystallographic iPP polymorphs,[45] and studied the independent effect of comonomer from the stereo defects on the formation of the γ phase.[7] These authors concluded that both ethylene and the *mrrm* stereo defects have essentially the same effect on the formation of this polymorph. In other words, both types of defects lead to the same crystallizable sequence lengths, which are the main parameters affecting both, the formation of the γ phase and the crystallization rate. Following this work the effect

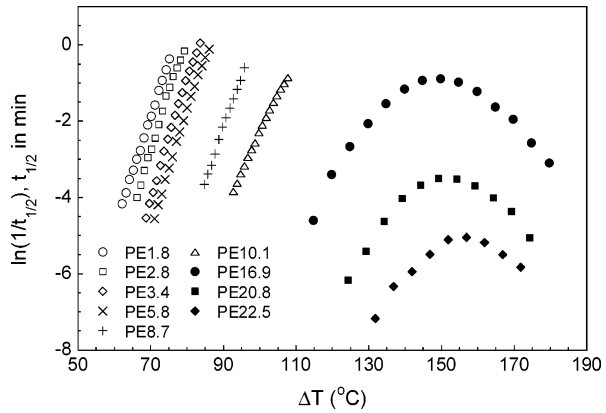

Figure 7. Overall crystallization rate expressed as $\ln(1/t_{1/2})$ as a function of undercooling ($T_m^o - T_c$). At a fixed undercooling the rate of crystallization decreases with increasing defects.

of the stereo (*mrrm*) and that of the ethylene defect on the rate should be equivalent.

A comparative assessment of crystallization rates between copolymers needs to be carried out at a constant undercooling ($\Delta T = T_m^o - T_c$). For this purpose the T_m^o of PEs were calculated theoretically using the Sanchez−Eby equilibrium relation.[3] Account was made for the nonuniform partitioning of the ethylene unit between the crystalline and noncrystalline regions, previously quantified by solid-state ^{13}C NMR.[9] The rate as $\ln(1/t_{1/2})$ is plotted vs ΔT in Figure 7. Clearly, the use of undercooling, based on T_m^o of the α or γ phase, does not bring the experimental rates to a common curve. There is not a fixed undercooling for which the rates could be compared for all copolymers. Crystallization in the allowable time scale shifts to progressively higher ΔT for PEs up to ∼15 mol %. In the range of ethylene where the rates can be compared at a fixed ΔT, this is either for PE1.8 to PE5.8 or for PE16.9 to PE22.5, the increase of ethylene causes a dramatic decrease in the crystallization rate of the copolymer. Over 250 times decrease in the rate is found for copolymers with ethylene contents changing from 15 to 20 mol %.

The displacement of the rates at higher ΔT with increasing ethylene in Figure 7 can be explained analyzing the fraction of crystallizable sequences (f_c*) that are allowed to participate in the isothermal crystallization of any given PE copolymer. f_c* is found summing over all crystallizable sequences longer than the critical length required to form a stable nucleus. To compute this fraction, the PE chain is considered a random copolymer of crystallizable and noncrystallizable units, thus accounting for the ethylene units that participate in the crystal and are included within crystallizable sequences. The crystalline ethylene fraction was calculated for all copolymers from solid-state NMR data and the X-ray crystallinities as described in previous works.[9,13] Average values incurred during slow crystallization for the concentration of ethylene in the crystal (X_C), the partitioning ratio defined as X_C over the ethylene concentration in the chain (X_B), the units of ethylene that are crystalline and the total content of crystalline units (X_A), both in mol %, are listed in Table 3. The partitioning ratio is similar for all PE copolymers (∼0.45), pointing to an ethylene uptake in the crystal that is proportional to the overall ethylene content.

With these data we estimate about one ethylene per 10 repeated isotactic units in the crystals of PE20.8; thus, the nature of these crystallites must be rather defective. The data of Table 3 also show that while increasing ethylene in the copolymers the content of ethylene in the crystal increases; however, from all ethylene units the percentage that is actually incorporated in the crystallites decreases from 30 to ∼10% with increasing comonomer due to the effect of defects restricting crystallinity.

The normalized fraction of sequences of *n* crystallizable units bounded at each end by a noncrystallizable unit is given as[46]

$$W_n = n(1 - X_A)^2 X_A^{n-1} \quad (4)$$

X_A is the fraction of crystallizable units. Equation 4 is plotted in Figure 8a as a function of crystalline sequence length ($n \times 0.217$ nm). The distribution becomes narrower with increasing comonomer, as pointed out by Crist et al.[47] From the W_n distribution, of interest are all *n* sequences with length equal or greater than the critical nucleus size (ξ*), the thickness of a nucleus stable at T_c. Only continuous crystallizable sequences of this length or greater can form crystallites, and to do so they must diffuse through the entangled melt to the nucleus front. A copolymer chain with a low concentration of sequences greater than ξ* will experience higher topological constraints in the melt and incur severely retarded crystallization. In the experimental time frame for rate measurement, this kinetic constraint is compensated by lowering the crystallization temperature to decrease the value of ξ* and hence increase the concentration of sequences $> \xi$*.

Estimates of ξ* can be obtained from nucleation theory. The free energy of forming a three-dimensional cylindrical nucleus comprising ρ molecules in cross-section and ξ repeating units in length is given by

$$\Delta G = 2\xi\sqrt{\pi\rho}\sigma + 2\rho\sigma_e - \xi\rho\Delta G_{copo} \quad (5)$$

σ and σ_e are the lateral and fold surface free energies, respectively. ΔG_{copo} is the free energy of fusion per repeating unit of the copolymer. In the case of comonomer inclusion in the crystal lattice, ΔG_{copo} can be expressed as[48]

$$\Delta G_{copo} = \Delta G_u - RT\left\{\epsilon\frac{X_C}{RT} + (1 - X_C)\ln\left[\frac{(1 - X_C)}{(1 - X_B)}\right] + X_C \ln\left(\frac{X_C}{X_B}\right)\right\} \quad (6)$$

ΔG_u is the free energy of fusion per repeating unit of an infinite molecular weight homopolymer, approximated by $\Delta H_u f(T_m^o - T)/T_m^o$. ΔH_u is the heat of fusion per repeating unit, T_m^o the equilibrium melting temperature of the homopolymer, and $f = 2T/(T_m^o + T)$ a correction factor to include higher order terms of the variation of the heat of fusion with temperature. X_B and X_C, listed in Table 3, have been defined earlier.

The dimensions of the critical nucleus size, ξ* and ρ*, are given by the saddle point of eq 5, $\xi^* = 4\sigma_e/\Delta G_{copo}$, and $\rho^* = 4\pi\sigma^2/\Delta G_{copo}^2$. The variation of ξ* as a function of ethylene for different crystallization temperatures is shown in Figure 8b. Of interest in this plot is the small variation in ξ* with increasing defects at the lowest T_cs or for very high undercoolings. For a comparative analysis of the available concentration of crystalline sequences in the copolymers, ξ* was taken at T_cs with the fastest observed crystallization rate in Figure 6. These ξ* values, shown as circles in Figure 8a, are 13.7, 12.8, 12.4, 10.4, 8.0, and 7.8 nm, for low to high ethylene respectively.

The concentration of *n* sequences of length $> \xi$* gives the fraction of sequences in the melt available for crystallization. This fraction, plotted in Figure 8c, indicates that while most sequences of PEs with low ethylene have the required length for nucleation, only 3.9% of the sequences of the copolymer with 16.9 mol % defects are equal or higher than the minimum required length. This value decreases to only 1.1% in the 20.8

Table 3. Crystallinity by WAXD and Data Related to the Partitioning of the Ethylene Units from Solid State ^{13}C NMR

defect[a]	X_B[b] (mol %)	crystallinity WAXD[c]	X_C (mol %)[d]	X_C/X_B[e]	crystalline ethylene (mol %)[f]	% of ethylenes that participate in crystallization[g]	X_A (mol %)[h]
ethylene	0.8	0.66	0.35	0.44	0.23	29	99.44
	2.2	0.65	1.03	0.46	0.67	30	98.47
	4.6	0.63	2.02	0.44	1.27	28	96.68
	7.5	0.58	3.10	0.42	1.80	24	94.33
	7.5	0.50	3.64	0.48	1.82	24	94.32
	14.7	0.30	6.83	0.46	2.05	14	87.35
	18.5	0.20	9.20	0.50	1.84	10	83.34

[a] Partitioning ratios for the *mrrm* stereo defect and for the 2,1-*erythro* regio defect are taken as 0.48 and 0.27, respectively.[13] Note that the value for the stereo defect is very similar to the ethylene value, predicting a similar effect of stereo and ethylene defects on crystallization rate in copolymers with equivalent distributions of these defects. The value for 2,1-*erythro* regio defect indicates that these defects are more restricted from the crystalline regions. [b] X_B is the number of moles of ethylene in 100 total moles of chain monomer units [c] Samples slowly cooled at 1 °C/min [d] X_C is the number of moles of ethylene in 100 mol of crystalline repeat units. [e] Partitioning ratio. [f] Moles of crystalline ethylene in 100 total moles of monomer units [g] Percentage of ethylene units that participate in crystallization [h] Moles of crystalline units in 100 total moles of chain monomer units

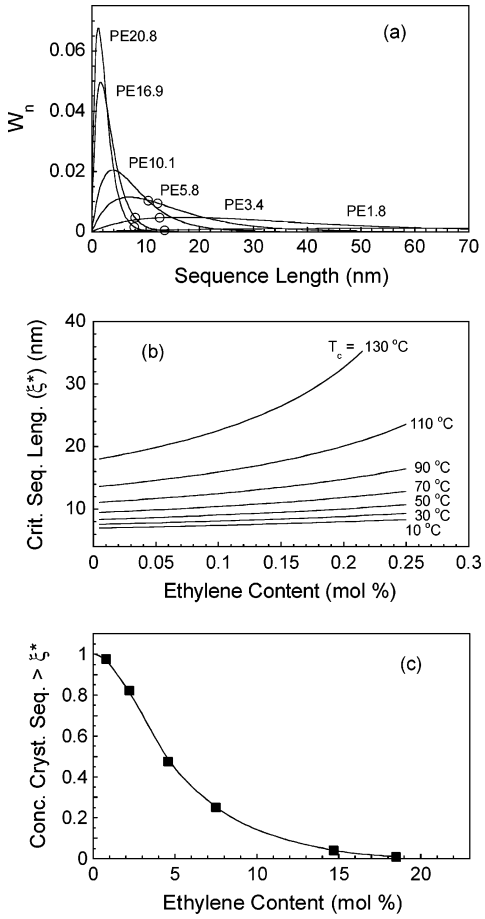

Figure 8. (a) Normalized fraction (W_n) of sequences of *n* crystallizable units bounded at each end by a noncrystallizable unit, calculated from eq 4 for the indicated PE copolymers. (b) Critical sequence length for nucleation (ξ^*) as a function of ethylene content calculated for increasing T_cs. (c) Fractional content of crystallizable sequences longer than ξ^*. Values of ξ^* were calculated for T_cs corresponding to the highest rates in Figure 6 and are shown as circles in part a.

mol % copolymer. Thus, classical nucleation points out that not only the undercooling needs to be adjusted from $\Delta T = 80$ to a $\Delta T \sim 150$, in order to observe the small number of crystallites formed from copolymers with >15 mol % ethylene, but the rate to gather these sequences to the growing front is limited by the small number suitable for crystallization. We see from the data of Figure 8c the direct effect of available crystallizable sequences on the overall crystallization rate.

The observation of the maximum crystallization rate brings the opportunity to model the bell shape of the rate of PE16.9, PE20.8, and PE22.5 vs T_c of Figure 6 with classical nucleation theory and the secondary nucleation approach for lamellar growth.[49] More recent approaches that diverge from the nucleation and growth path of crystallization have provided a mechanism to test experimental linear growth rates.[50] Moreover, data for overall rates cannot be analyzed yet with this model.[51,52] The advantage of fitting the complete crystallization curves with theoretical models is that the results provide an independent set of T_m^o of the copolymers to probe adherence with those calculated from the equilibrium relation. Independent T_m^o can further assess the effect of increasing ethylene on the crystallization rate at a constant undercooling. The classical Avrami equation is first written using parameters appropriate to the crystallization of PE copolymers with >8 mol % ethylene ($n = 4$).[53]

$$X(t) = 1 - \exp\left(-\frac{\pi}{3} G^3 \dot{N} t^4\right) = 1 - \exp(-kt^4) \qquad (7)$$

where $\dot{N}$ is the constant nucleation rate and G is the linear growth rate. Writing this equation for $t_{1/2}$ gives

$$\ln\left(\frac{1}{t_{1/2}}\right) = \frac{1}{4}\ln\left(\frac{\pi}{3\ln(2)}\right) + \frac{1}{4}\ln(\dot{N}) + \frac{3}{4}\ln(G) \qquad (8)$$

The analysis of experimental data with eq 8 requires expressions for $\dot{N}$ and G. The Turnbull and Fischer equation[54] is used to represent the dependence of $\dot{N}$ with temperature:

$$\dot{N} = N_o \exp\left(-\frac{E_D}{RT_c} - \frac{\Delta F_n^*}{RT_c}\right) \qquad (9)$$

In this equation, E_D is the activation energy for segmental transport across the liquid-crystal boundary, and ΔF_n^* the free energy change to form a stable nucleus. Since the experimental data are obtained at temperatures relatively close to T_g, E_D is expressed with the Vogel−Fulcher activation energy term for viscous flow of amorphous polymers, $U^*T_c/(T_c - T_g + C_2)$, where C_2 is a constant, and $T_g + C_2 = T_\infty$, represents the temperature below which the required segmental motion becomes infinitely slow. The form of ΔF_n^* depends on the geometry of the nucleus considered. For a three-dimensional nucleus (cylindrical geometry) ΔF_n^* is given as[55]

$$\Delta F_n^* = \frac{8\pi\sigma_e\sigma^2}{\Delta G_u^{\,2}} \qquad (10)$$

For lamellar growth via coherent molecular deposition on a

surface[49]

$$G = G_o \exp\left(-\frac{E_D}{RT_c} - \frac{\Delta F_c^*}{RT_c}\right) \quad (11)$$

where ΔF_c^* is associated with the free energy term for the formation of a nucleus on a pre-existing surface.

$$\Delta F_c^* = \frac{4\sigma\sigma_e T_m^o}{\Delta H_u \Delta T f} \quad (12)$$

With the assumption of constant interfacial free energies during nucleation and growth, substitution of eqs 9−12 into eq 8 with the Vogel−Fulcher activation energy term results in the following rate expression:

$$\ln\left(\frac{1}{t_{1/2}}\right) = C - \frac{U^*}{R(T_c - T_g + C_2)} - \frac{K_{n,3D}}{4T_c \Delta T^2 f^2} - \frac{3K_g}{4T_c \Delta T f} \quad (13)$$

where $C = {}^1/_4 \ln(\pi G_o^3 N_o/(3 \ln 2))$ for 3-D primary nucleation, and $K_{n,3D}$ and K_g are defined as

$$K_{n,3D} = \frac{8\pi\sigma_e\sigma^2 T_m^{o\,2}}{R\Delta H_u^{\,2}}, \quad K_g = \frac{4\sigma\sigma_e T_m^o}{R\Delta H_u} \quad (14)$$

Unknown parameters in eq 13 are as follows: C, U^*, C_2, and T_m^o. However, the precise observation of the maximum in the rate enables to reduce mathematically the unknown parameters to three via

$$\frac{\partial}{\partial T}\left(\ln\left(\frac{1}{t_{1/2}}\right)\right)_{T_c = T_{max}} = 0 \quad (15)$$

where T_{max} is the temperature at the rate maxima. After differentiation, U^* is expressed as

$$U^* = R(T_1 - T_g + C_2)^2\left(\frac{K_{n,3D}}{16} W + \frac{3}{4} K_g Y\right) \quad (16)$$

In this equation W and Y are given as

$$W = \frac{(T_m^o + T_{max})\{4T_m^o T_{max} - 3(T_m^{o\,2} - T_{max}^{\,2})\}}{T_{max}^{\,4}(T_m^o - T_{max})^3} \quad (17)$$

and

$$Y = \frac{(T_m^o T_{max} - T_m^{o\,2} + T_{max}^{\,2})}{T_{max}^{\,3}(T_m^o - T_{max})^2} \quad (18)$$

Substitution of U^* (eqs 16−18) in eq 13 allows fits of the experimental data with three adjustable parameters (C_2, C, and T_m^o). We attempted to reduce the degrees of freedom to two parameters using the so-called universal values for C_2 (30 or 51.6°); however, the experimental data could not be fitted with these values. The surface free energies used in the calculations were estimated from the relation of σ_e with ethylene content obtained in a previous work.[3] The values of σ and ΔH_u used are 13.5 erg/cm^2 for the former and 209 (α) and 190 J/g (γ) for the latter, respectively. The results are listed in Table 4 and shown as continuous lines in Figure 6. The T_m^o values obtained from the best fits are compared in Figure 9 with the equilibrium values and with those obtained by Dimeska and Phillips[56] from an analysis of the crystallization at different pressures of two

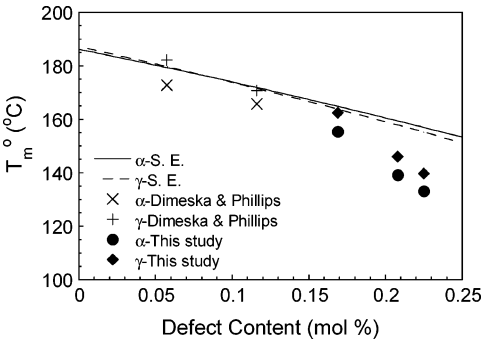

Figure 9. Equilibrium melting temperatures vs defect content for PE copolymers. Shown are values for the α and γ phases calculated from the Sanchez−Eby equation,[3] those obtained by Dimeska and Phillips,[56] and values from this study.

Table 4. Best Fitting Parameters of Experimental Rates with Equation 13 and the Sum of the Squared Differences, SSD, and T_m^o Calculated with the Sanchez−Eby Equation[3]

	T_m^o (°C)	T_m^o(S. E.) (°C)	C (min^{-1})	C_2 (K)	U^* (cal/mol)	SSD
			Alpha			
PE16.9	155.3	164.8	50.1	129.7	7220	0.046
PE20.8	139.1	159.3	53.5	131.2	8214	0.067
PE22.5	132.9	156.9	50.9	134.9	7699	0.056
			Gamma			
PE16.9	162.4	163.7	53.7	130.0	7359	0.051
PE20.8	145.9	157.7	56.8	131.2	8052	0.077
PE22.5	139.6	155.1	54.4	133.5	7553	0.056

Ziegler−Natta PEs fractions. Considering that these three methods are independent and that there is a high correlation between parameters such as ΔH_u, σ_e, and T_m^o, we find a reasonable agreement between the three data sets for concentration of defects up to ∼15 mol %. For copolymers with >15 mol %, the T_m^o obtained from the fits are 10−25 °C lower than the theoretical values. One possible explanation for this divergence, among others, is that ΔH_u could be significantly altered for the defective crystallites formed at high comonomer level. The C_2 values obtained from the best fits (∼130 K) are higher than the ∼50 K usually taken for the temperature range below T_g where all motion associated with viscous flow ceases. A higher C_2 value indicates a stronger departure from T_g to find infinitely slow motion of these copolymers, perhaps due to the increased free volume conferred by the ethylene units.

Given that in a wide range of ethylene the values of T_m^o from two independent assessments are in reasonable agreement, we conclude that the trend of Figure 7 is correct, confirming the decrease in crystallization rate with increasing ethylene content. Since the ethylene and the stereo defects have shown a similar partitioning ratio, and equivalent effect on the formation of the γ polymorph,[1,7] the same conclusion is drawn for the effect of stereo defects on the crystallization rate of iPPs, thus contradicting the conclusion reached in a preceding work.[11] As mentioned, the Hoffman−Weeks extrapolation, is not applicable to iPP random copolymers or iPPs with stereo defects for reasons detailed in earlier studies.[3,12]

Crystallographic Polymorphs. It is well-known that the formation of the γ phase is favored in polypropylenes and propylene copolymers with chain microstructures characterized by short crystallizable sequences runs, and under slow crystallization conditions (increasing T_c). Any defect that interrupts the isotactic regularity of the iPP chain (the common stereo, head to head types, or comonomer units) leads to higher contents of the γ polymorph. Furthermore, it has been shown in at least

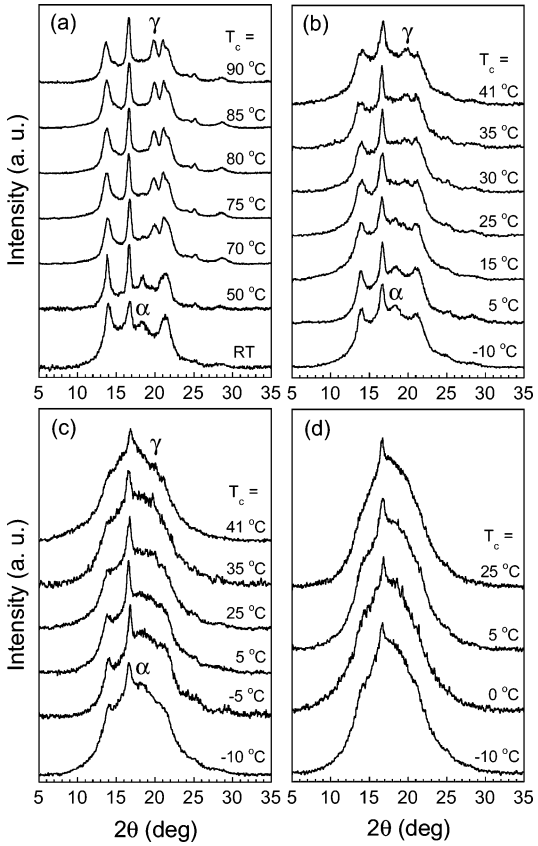

Figure 10. WAXS diffractograms of (a) PE10.1, (b) PE16.9, (c) PE20.8, and (d) PE22.5 crystallized at the indicated temperatures. Reflections corresponding of the α and γ polymorphs are indicated. Diffractograms of copolymers crystallized at T_c below 15 °C were obtained at the crystallization temperature using a Peltier cell.

two previous works that iPPs with defects that are better tolerated in the lattice develop crystallites with lower contents of the γ phase due to their longer crystallizable sequence lengths.[1,7] The observed differences in polymorphic behavior of propylene ethylene and propylene butenes (PB) with matched comonomer content reflect this effect.[1,7] Since the butene unit is more effectively incorporated in the crystal, copolymers with <15 mol % butene develop less γ than analog propylene ethylenes. At >∼15 mol % a large expansion of the lattice from the butene incorporation produce inequalities in the length of the *a* and *c* axes, a requirement for the epitaxial growth of the γ phase, consequently γ is no longer formed in these PB copolymers.[7]

In De Rosa et al.'s comparative work,[7] the highest ethylene content studied was 13.1 mol %, and the polymorphism was studied in a relatively high range of crystallization temperatures (>65 °C), thus leading to 100% γ at all T_c investigated. From these data one may conclude that PEs with >13 mol % will not develop α phase. However, given that changes in the crystallographic packing beyond the usual mixed α/γ phases have been found in PB and PH copolymers at contents >15 mol %,[4,5,7] we have investigated the polymorphism of PEs in a range of ethylene from ∼15 up to 21 mol %. Furthermore, the effect of crystallization kinetics on the formation of the γ phase is studied over the whole range of T_cs, in the diffusion as well as nucleation controlled crystallization ranges.

Diffractograms of copolymers in the high range of ethylene are given in Figure 10 for isothermal crystallization temperatures changing from −10 to +90 °C. The diffractograms of PE16.9 and PE20.8 crystallized from −10 to +15 °C were obtained at

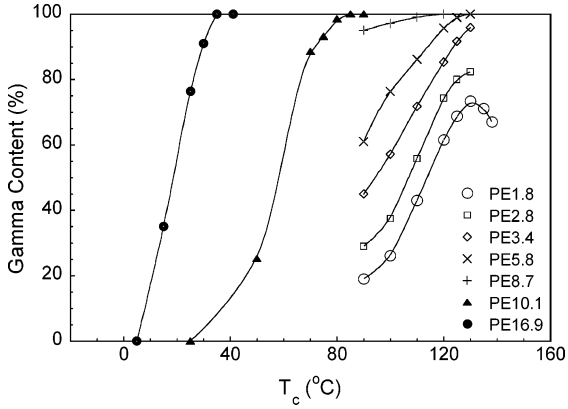

Figure 11. Percentage of γ polymorph as a function of crystallization temperature for propylene ethylene copolymers.

the isothermal crystallization temperatures using a Peltier attachment for subambient crystallization. The change from pure α to γ with increasing T_c is observed in PE10.1, PE16.9, and PE20.8 as well. However, discrimination between both phases is not possible from the weak reflections of PE22.5, due to the relatively low crystallinity and the defective nature of the crystallites that accommodate high ethylene contents at this comonomer level. Interestingly, the type of crystallographic form that develops in PEs > 10 mol % ethylene depends on whether crystallization takes place to the right or to the left of T_{max}. At temperatures to the left of T_{max}, PE16.8 develops only the α polymorph, while at T_cs to the right of T_{max}, γ is preferentially formed. The increase of γ content with T_c has been discussed as a competition between kinetic and thermodynamic driving forces in developing each crystallographic phase.[1,57,58] It was postulated that while α is the kinetically favored structure, the γ form is thermodynamically more stable; hence, its formation is favored at T_cs approaching the equilibrium value. In support of this postulate, the free energy to form the γ phase was found lower than for the α.[59] The thermodynamic argument still holds to interpret the polymorphic change of PEs > 15 mol % below and above T_{max} (γ increases with lowering undercooling); however, the kinetic one does not apply for the formation of pure α phase at T_cs to the left of T_{max}. With decreasing T_c, the α phase is still the preferred structure; however, the kinetics of the formation of this phase are as slow as those to the right of T_{max} where high contents of γ develop. Clearly, at crystallization temperatures for which segmental motion is more restricted and governs the development of the crystalline state, the γ phase is not formed. Hence, it appears that in addition to short crystallizable sequences, considerable molecular diffusion is required to propagate the unique nonparallel molecular structure of the γ form. On these grounds, increased segmental mobility arguments also explain the increase of γ phase with pressure observed in the homopolymer and fractions from a Ziegler−Natta based propylene ethylene copolymer.[56,60]

The variation of γ content with increasing T_c is given in Figure 11 where data for lower ethylene content of an earlier work,[1] are also included to illustrate the variation of γ in a large concentration of ethylene. The intensity and resolution of the α and γ polymorphs in the patterns of PE20.8 and PE22.5 (Figure 10, parts c and d) is too low for meaningful quantitative data, and are not included. We learn from Figures 10 and 11 that both polymorphs develop in PEs up to very high contents of ethylene (∼20 mol %) and their relative content follows the same variation with T_c. The most relevant difference is the range of T_cs where both polymorphs coexist. This range is relatively broad for ethylene contents <∼10 mol % but becomes narrow

for ethylene ≥10 mol % due to the restrictions of formation of γ in the T_c range of diffusion-controlled crystallization.

Morphology. The possibility of following the crystallization of PE copolymers >10 mol % in the nucleation controlled range as well as in the temperature interval where crystallization is governed by segmental diffusion, offers the opportunity to study the crystalline morphologies that evolve with increasing undercooling in both regimes, and address the role of nucleation or transport driven kinetics in the type of crystals formed. In contrast, the lamellar morphologies of copolymers with <10 mol % could only be studied for crystallites formed in the nucleation driven range given their fast crystallization with increasing undercooling.[2] Isothermally crystallized PE copolymers with <10 mol % ethylene display lamellar growth habits that are characteristic of the epitaxial models given for γ crystals branching at high tilt angles from α surfaces.[61,62] Conforming to this model, it was found that α lamellae growing in the direction of the radial axis of the spherulite are replaced in γ-rich copolymers with a dense array of short lamellae transverse or tilted to the main structural growth axis.[2]

Representative AFM images of the lamellar morphologies developed in PE16.9, PE20.8 and PE22.5 with increasing T_c are given in Figure 12. In the nucleation controlled T_c range, for PE20.8 and PE22.5 at $10 < T_c < 30$ °C where pure or predominantly γ crystals are formed, the lower melt viscosity enables chain mobility to gather crystalline sequences that propagate long and relatively straight lamellae, radiating from a common center and forming large and open sheaflike structures. The lamellae appear with limited branching as is characteristic of the γ phase,[63] and resemble the axialitic structure of polyethylenes and other systems formed at very low undercoolings.[64] For homopolymers, slow growth at low ΔT is a consequence of the high-energy barrier for surface nucleation. However, even at relatively high ΔT (see Figure 7), PE copolymers develop similar axialitic structures due to the low concentration of sequences that are available for crystallization in this comonomer range. Crossed-hatched lamellae are only found in copolymers with higher crystallinity, for example, in the center of the aggregates formed after crystallizing PE16.9 at $T_c = 30-40$ °C where a mixture of α and γ crystals develop.

The number of nuclei that evolve as axialites increases with decreasing T_c as the energy barrier for primary nucleation decreases; however, as T_c decreases further and enters the diffusion-controlled range, axialitic aggregates are no longer formed; numerous short rodlike lamellae develop randomly instead. With increasing ethylene this is observed for T_cs < 20, 10, and 5 °C for the copolymers shown in Figure 12. Images of PE16.9 crystallized at $T_c < 30$ °C (not shown) were granular and devoid of lamellar details. For PE20.8 and PE22.5 at T_cs approaching T_g ($T_c \leq 5$ °C), a high undercooling provides a dense population of nucleating sites while the increased viscosity restricts transport of the crystallizable sequences, limiting lamellar growth, as observed in the micrographs. Although the difference in molecular weights between these two copolymers causes dramatic differences in their crystallization rates, as shown earlier, their crystalline morphology is essentially identical. Notice that the increased molar mass does not provide blockier lamellae as would be expected for PE22.5, compared to the lower molar mass PE20.8, if lamellar growth in these system progresses via an intermediate mesomorphic structure of the type recently postulated.[52,52]

In spite of the large range of T_cs analyzed, the lamellar thicknesses measured from the AFM images average ~86 ± 8 Å with small variations among the copolymers or with increasing T_c (Table 5). The most general deduction that can be made from the negligible increase of thickness with T_c is in reference to the high undercoolings at which crystallization takes place for copolymers with >10 mol % ethylene. All experimental evidence for crystallite thicknesses of homopolymers reflect a decrease with increasing ΔT, leveling off to constant values at the lowest T_cs.[65] While the iPP homopolymer crystallizes at ΔT lower than ~50 °C, we see from Figure 7 that ΔT for these copolymers is >100 °C; thus, the small variation in thicknesses is explained by the required large ΔT, and follows the behavior of homopolymers under comparable undercoolings. Furthemore, as seen in Figure 8b, the required thickness to form a stable nucleus at the lowest crystallization temperatures is similar for all copolymers studied. Hence, nucleation theory also explains the observed small difference in thicknesses for these PE copolymers when the nucleus size is taken as characteristic of the fully developed crystallite.

The variation of crystallite aggregates with increasing ethylene in the whole series (1.8−22.5 mol % defects) crystallized at 23 °C is remarkably similar to the features observed in random propylene 1-hexene copolymers (PH), especially at the ~20 mol % level of comonomer.[4] Even the change of size of aggregates with increasing comonomer is similar in both series. Observation of sheaflike morphologies in PH copolymers by Poon et al.[4] was directly associated with the participation of the 1-hexene units in the crystallites and the development of a different crystallographic phase (a trigonal structure) at high levels of 1-hexene comonomer.[4,6] However, as shown in Figure 12, PEs develop identical morphologies as PHs, yet a different crystallographic phase is not formed. It is then concluded that the development of sheaflike or axialitic morphology is not a consequence of a change in crystallographic pattern; rather it must reflect a crystallization mechanism of these copolymers enabled by a high participation of the comonomer in the formation and propagation of the crystalline structure.

The axialitic morphologies observed in PEs and PHs with >15 mol % comonomer are not developed by random copolymers with comonomers excluded from the lattice, such as the 1-octene unit. For example, AFM images of propylene 1-octene copolymers in a wide range of comonomer content reveal that lamellae-like crystallites are no longer formed at 1-octene contents greater than ~15 mol %.[10] As already mentioned, crystallization entitles, first, availability of a number of sequences sufficiently long to form stable crystallites, and second, a mechanism that enables packing of these sequences throughout the entangled melt. Compared to analogous PEs or PHs, the crystalline sequence length, and number of crystalline sequences decreases in PO copolymers; additionally, once long sequences are pinned to crystallites, restrictions on transport of additional sequences to the propagating crystal surface limits the feasibility of the crystallization process at high levels of comonomer. As a consequence, lamellar-like crystallites are only observed at relatively low concentrations of 1-octene or low concentrations of any other comonomer rejected from the lattice.[66,67]

Propagation of relatively thick long lamellae, as seen for PE22.5 in Figure 12 ($T_c = 10-23$ °C) is only feasible if continuous long chain segments participate in the crystal. An estimate of the sequence length along the "*c*" axis of the crystallite can be made from the NMR-based concentration of ethylene in the crystal (9.2 mol % for PE20.8) and the crystallite thickness (~85 Å). We calculate for this copolymer that the stems of the crystallites contain an average of four sequences, each with ~10 isotactic units bounded by ethylene units at the

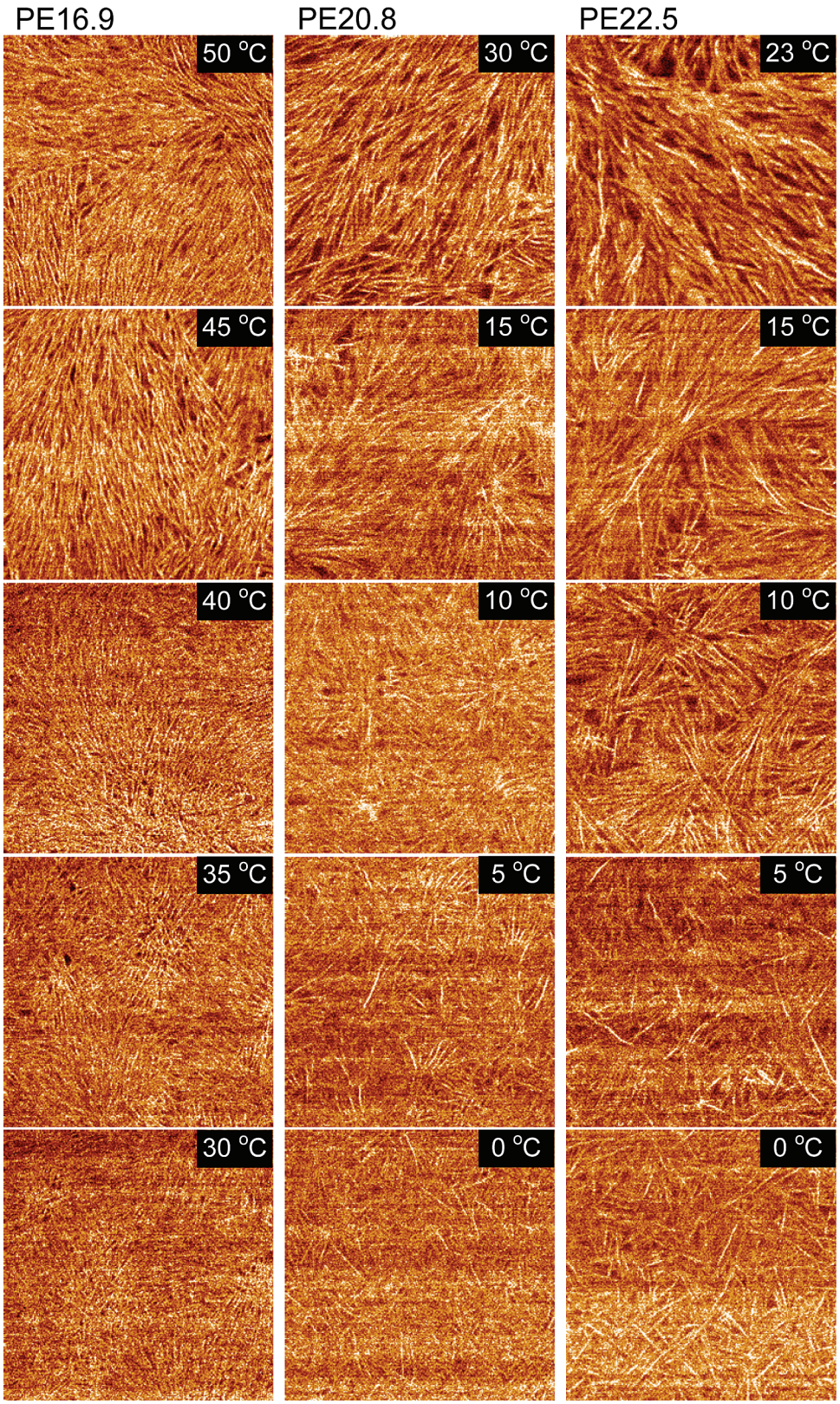

Figure 12. AFM phase images (1.5 × 1.5 μm^2) for PE16.9, PE20.8, and PE22.5 crystallized at the temperatures indicated.

ends. These relatively short sequences support packing comonomer rich segments in these copolymers, and explain the departure of T_m^o from the equilibrium value in Figure 9. The argument of packing and folding chain segments with a relatively high content of ethylene to propagate lamellar crystallites parallels recent works in precisely branched polyolefins that were found to crystallize as homopolymers, with no discrimination in the partitioning of the branch, provided the branch is accommodated in the crystal.[68] We thus postulate that the morphology observed in PEs and PHs copolymers at high comonomer levels correlates with a change in the mechanism of developing the crystalline structure of iPP random copolymers. While crystalline sequence selection is the major driving force at the low comonomer levels, the ability to accommodate the comonomer in a stable lattice leads to the development of crystallinity when the distance between con-

Table 5. Lamellar Thicknesses Measured from AFM Images for PE Crystallites Formed at Increasing T_cs

PE16.9		PE20.8		PE22.5	
T_c (°C)	thickness (nm)	T_c (°C)	thickness (nm)	T_c (°C)	thickness (nm)
50	8.4 ± 0.7	35	8.5 ± 0.7	23	9.4 ± 0.7
45	8.6 ± 0.6	30	8.2 ± 0.6	15	8.6 ± 0.5
40	8.2 ± 0.6	23	8.7 ± 0.6	10	9.0 ± 0.6
35	8.4 ± 0.8	15	8.2 ± 0.8	5	8.9 ± 0.7
30	7.9 ± 0.5	10	8.4 ± 0.7	0	9.2 ± 0.8
		5	8.7 ± 0.8		
		0	8.1 ± 0.6		

secutive comonomer units in the iPP chain decreases. Moreover, the loss of iPP-based crystallinity at PE levels of 30−50 mol %[8,69] infers an obvious limit in the content of cocrystallizable counits that can be incorporated in a stable iPP isomorphous lattice.

Conclusions

A microstructural analysis of the ^{13}C NMR triad distribution of sequences pertaining to ethylene in a series of metallocene PE copolymers, is consistent with predictions from Bernoullian models. Major deviations from this pattern were not found in copolymers with ethylene up to 20 mol %. The values of the product of reactivity ratio are significantly lower than those of copolymers synthesized with a Ziegler−Natta catalyst reflecting a more random distribution.

PE copolymers with high ethylene contents (>10 mol %) crystallize in a T_c range close to T_g. The maximum of the temperature-dependent crystallization rate (T_{max}) was experimentally obtained for these copolymers and the temperature coefficient of the rate adequately modeled with nucleation and growth theory. Values of T_m^o obtained from the best fits and those calculated from equilibrium relations were similar for PEs with <15 mol % ethylene. At a fixed undercooling, the overall crystallization rates of PEs decrease with increasing ethylene. Since ethylene and the stereo defects have an analogous partitioning between crystalline and noncrystalline regions, and develop similar contents of γ phase, it is concluded that the same crystallization rate dependence of the ethylene defect holds for the stereo defect. The restraints on sequence participation, which is unique to random copolymers, influence the time scale of the crystallization. In the range of T_c approaching T_g, for relatively high ethylene content, the effect of segmental dynamics in developing the semicrystalline structure is very pronounced as evidenced by a dramatic decrease of the crystallization rate with molar mass.

Both α and γ polymorphs develop in PEs in the whole range of ethylene content analyzed (up to 21 mol %). The content of γ phase of PEs with >7 mol % comonomer follows, with increasing T_c, the pattern observed for the lower ethylene copolymers. The γ phase does not develop at temperatures at which crystallization is governed by segmental diffusion (temperatures below T_{max}). This observation reveals that a significant segmental mobility is required, in addition to a chain microstructure with short crystallizable sequences, to develop the γ polymorph.

Copolymers with >15 mol % ethylene form long lamellae with the same sheaflike crystalline structures found in propylene 1-hexene copolymers with matched comonomer contents, yet the crystalline unit cell is unchanged in PEs. Clearly a change in unit cell and higher crystallinities are not required for PEs to develop axialitic structures at high ethylene contents. We associate the formation of sheaflike morphologies with a mode of crystallization that requires less preferential partitioning of the comonomer units. When the i-PP counit can be accommodated in a stable lattice, propagation of relatively thick, long lamellae-like crystals requires the participation and folding of long chain segments and, thus, the participation of high contents of the counit.

Acknowledgment. Funding of this work by the National Science Foundation, Grant DMR-0503876, is gratefully acknowledged. We also gratefully acknowledge the assistance of Dr. E. Lockner of MARTECH at FSU with X-ray measurements, F. Nozirov with solid-state NMR, and URP student S. Warnock for assistance with collection of DSC data.

Supporting Information Available: Text giving additional experimental details and figures showing diffractograms of PE16.9 obtained at increasing temperatures, variation with temperature reflecting volume expansion of radial coils, and extraction of crystalline diffractogram and peak deconvolution to obtain crystallinity and polymorphic content, representative examples of cross-section profiles and phase images, and solid-state ^{13}C NMR crystal spectra. This material is available free of charge via the Internet at http://pubs.acs.org.

References and Notes

(1) Hosier, I. L.; Alamo, R. G.; Esteso, P.; Isasi, J. R.; Mandelkern, L. *Macromolecules* **2003**, *36*, 5623.
(2) Hosier, I. L.; Alamo, R. G.; Lin, J. S. *Polymer* **2004**, *45*, 3441.
(3) Alamo, R. G.; Ghosal, A.; Chatterjee, J.; Thompson, K. L. *Polymer* **2005**, *46*, 8774.
(4) Poon, B.; Rogunova, M.; Hiltner, A.; Baer, E.; Chum, S. P.; Galeski, A.; Piorkowska, E. *Macromolecules* **2005**, *38*, 1232.
(5) De Rosa, C.; Auriemma, F.; Corradini, P.; Tarallo, O.; Dello Iacono, S.; Ciaccia, E.; Resconi, L. *J. Am. Chem. Soc.* **2006**, *128*, 80.
(6) Lotz, B.; Ruan, J.; Thierry, A.; Alfonso, G. C.; Hiltner, A.; Baer, E.; Piorkowska, E.; Galeski, A. *Macromolecules* **2006**, *39*, 5777.
(7) De Rosa, C.; Auriemma, F.; Ruiz de Ballesteros, O.; Resconi, L.; Camurati, I. *Macromolecules* **2007**, *40*, 6600.
(8) Stephens, C. H.; Poon, B. C.; Ansems, P.; Chum, S. P.; Hiltner, A.; Baer, E. *J. Appl. Polym. Sci.* **2006**, *100*, 1651.
(9) Alamo, R. G.; Vanderhart, D. L.; Nyden, M. R.; Mandelkern, L. *Macromolecules* **2000**, *33*, 6094.
(10) Poon, B.; Rogunova, M.; Chum, S. P.; Hiltner, A.; Baer, E. *J. Polym. Sci., Polym. Phys. Ed.* **2004**, *42*, 4357.
(11) De Rosa, C.; Auriemma, F.; Resconi, L. *Macromolecules* **2005**, *38*, 10080.
(12) Crist, B. *Polymer* **2003**, *44*, 4563.
(13) VanderHart, D. L.; Alamo, R. G.; Nyden, M. R.; Kim, M.-H.; Mandelkern, L. *Macromolecules* **2000**, *33*, 6078.
(14) Mehta, A. K.; Chen, M. C.; McAlpin, J. J. In *Metallocene-Catalyzed Polymers: Materials, Properties, Processing, and Market*; Benedikt, G. M., Goodall, B. L., Eds.; Plastic Design Library: New York, 1998; p 261.
(15) Kaminsky, W.; Külper, K.; Brintzinger, H. H.; Wild, F. R. W. P. *Angew. Chem., Int. Ed. Engl.* **1985**, *24*, 6.
(16) Randall, J. C. *J. Macromol. Sci.—Rev. Macromol. Chem. Phys.* **1989**, *C29*, 201.
(17) Hayashi, T.; Inoue, Y.; Chujo, R.; Asakura, T. *Polymer* **1988**, *29*, 1848.
(18) Hayashi, T.; Inoue, Y.; Chujo, R.; Asakura, T. *Polym. J.* **1988**, *20*, 895.
(19) Tritto, I.; Fan, Z.-Q.; Locatelli, P.; Sacchi, M. C. *Macromolecules* **1995**, *28*, 3342.
(20) Busico, V.; Cipullo, R. *Prog. Polym. Sci.* **2001**, *26*, 443.
(21) Mizuno, A.; Tsutsui, T.; Kashiwa, N. *Polymer* **1992**, *33*, 254.
(22) Tsutsui, T.; Ishimaru, N.; Mizuno, A.; Toyota, A.; Kashiwa, N. *Polymer* **1989**, *30*, 1350.
(23) Alamo, R. G.; Blanco, J. A.; Agarwal, P.; Randall, J. C. *Macromolecules* **2003**, *36*, 1559.
(24) Brückner, S.; Meille, S. V. *Nature* (*London*) **1989**, *340*, 455.
(25) Turner-Jones, A.; Aizlewwod, J. M.; Beckett, D. R. *Makromol. Chem.* **1964**, *75*, 134.
(26) GRAMS. Thermo Fisher Scientific, 2006.
(27) Wang, H. P.; Ansems, P.; Chum, S. P.; Hiltner, A.; Baer, E. *Macromolecules* **2006**, *29*, 1488.
(28) Alamo, R. G.; Mandelkern, L. *Thermochim. Acta* **1994**, *238*, 155.

(29) Shih, C.-K.; Su, A. C. L. in *Thermoplastic Elastomer- A Comprehensive Review*; Legge, N. R., Schroeder, H. E., Holden, G., Eds.; Hanser Publishers: New York, 1987; p 98 [Chapter 5].
(30) Shin, Y.-W.; Uozumi, T.; Terano, M.; Nitta, K.-H. *Polymer* **2001**, *42*, 9611.
(31) Brintzinger, H. H.; Fischer, D.; Mülhaupt, R.; Rieger, B.; Waymouth, R. M. *Angew. Chem., Int. Ed. Engl.* **1995**, *34*, 1143.
(32) Kakugo, M.; Naito, Y.; Mizunuma, K.; Miyatake, T. *Macromolecules* **1982**, *15*, 1152.
(33) Carman, C. J.; Harrington, R. A.; Wilkes, C. E. *Macromolecules* **1977**, *10*, 536.
(34) Randall, J. C. *Polymer Sequence Determination C-13 NMR Method*; Academic Press: New York, 1977.
(35) Liu, Y.; Bo, S.; Zhu, Y.; Zhang, W. *J. Appl. Polym. Sci.* **2005**, *97*, 232.
(36) Randall, J. C. *J. Polym. Sci., Polym. Chem. Ed.* **1998**, *36*, 1527.
(37) Feng, Y.; Hay, J. N. *Polymer* **1998**, *39*, 6589.
(38) Hosoda, S.; Hori, H.; Yada, K.; Nakahara, S.; Tsuji, M. *Polymer* **2002**, *43*, 7451.
(39) Arnold, M.; Henschke, O.; Knorr, *J. Macromol. Chem. Phys.* **1996**, *197*, 563.
(40) Supaphol, P.; Spruiell, J. E. *Polymer* **2001**, *42*, 699.
(41) De Rosa, C.; Auriemma, F.; Paolillo, M.; Resconi, L.; Camurati, I. *Macromolecules* **2005**, *38*, 9143.
(42) Alamo, R. G.; Mandelkern, L. *Macromolecules* **1991**, *24*, 6480.
(43) Berry, G. C.; Fox, T. G. *Adv. Polym. Sci.* **1968**, *5*, 261.
(44) Alamo, R. G.; Kim, M.-H.; Galante, M. J.; Isasi, J. R.; Mandelkern, L. *Macromolecules* **1999**, *32*, 4050.
(45) De Rosa, C.; Auriemma, F.; Circelli, T.; Waymouth, R. M. *Macromolecules* **2002**, *35*, 3622. De Rosa, C.; Auriemma, F.; Circelli, T.; Longo, P.; Boccia, A. C. *Macromolecules* **2003**, *36*, 3465. De Rosa, C.; Auriemma, F.; Spera, C.; Talarico, G.; Tarallo, O. *Macromolecules* **2004**, *37*, 1441. De Rosa, C.; Auriemma, F.; Spera, C.; Talarico, G.; Gahleitner, M. *Polymer* **2004**, *45*, 5875.
(46) Flory, P. J. *J. Chem. Phys.* **1949**, *17*, 223.
(47) Crist, B.; Claudio, E. S. *Macromolecules* **1999**, *32*, 8945.
(48) Sanchez, I. C.; Eby, R. K. *Macromolecules* **1975**, *8*, 638.
(49) Hoffman, J. D.; Davis, G. T.; Lauritzen, J. I., Jr. In *Treatise on Solid State Chemistry*; Hannay, N. B., Ed.; Plenum Press: New York, 1976; Vol. 3; Chapter 7.
(50) Cho, T. Y.; Stille, W.; Strobl, G. *Macromolecules* **2007**, *40*, 2596.
(51) Strobl, G. *Eur. Phys.* **2005**, *18*, 295.
(52) Sirota, E. B. *Macromolecules* **2007**, *40*, 1043.
(53) Chiary, Y. L.; Vadlamudi, M.; Jeon, K.; Chella, R.; Alamo, R. G. *Polymer* **2007**, *48*, 3170.
(54) Turnbull, D.; Fischer, J. C. *J. Chem. Phys.* **1949**, *17*, 7.
(55) Mandelkern, L.; Fatou, J. G.; Howard, C. *J. Phys. Chem.* **1964**, *68*, 3386.
(56) Dimeska, A.; Phillips, P. J. *Polymer* **2006**, *47*, 5445.
(57) Alamo, R. G.; Kim, M.-H.; Galante, M. J.; Isasi, J. R.; Mandelkern, L. *Macromolecules* **1999**, *32*, 4050.
(58) Meille, S. U.; Ferro, D. R.; Brückner, S. *Macrom. Symp.* **1995**, *89*, 499.
(59) Ferro, D. R.; Brückner, S.; Meille, S. V.; Ragazzi, M. *Macromolecules* **1992**, *25*, 5231.
(60) Mezghani, K.; Phillips, P. J. *Polymer* **1997**, *23*, 5725.
(61) Lotz, B.; Graff, S.; Wittmann, J. C. *J. Polym. Sci., Polym. Phys. Ed.* **1986**, *24*, 2017.
(62) Meille, S. V.; Brückner, S.; Porzios, W. *Macromolecules* **1990**, *23*, 4114.
(63) Thoman, R.; Wang, C.; Kressler, J.; Mülhaupt, R. *Macromolecules* **1996**, *29*, 8425.
(64) Bassett, D. C. *Principles of Polymer Morphology*; Cambridge University Press: New York, 1981.
(65) Mandelkern, L. *J. Phys. Chem.* **1971**, *75*, 3909.
(66) Bensason, S.; Minick, J.; Moet, A.; Chum, S.; Hiltner, A.; Baer, E. *J. Polym. Sci., Polym. Phys. Ed.* **1996**, *34*, 1301.
(67) Voigt-Martin, I. G.; Alamo, R.; Mandelkern, L. *J. Polym. Sci., Polym. Phys. Ed.* **1986**, *24*, 1283.
(68) Boz, E.; Wagener, K. B.; Ghosal, A. K.; Fu, R.; Alamo, R. G. *Macromolecules* **2006**, *39*, 4437.
(69) Guerra, G.; Ruiz de Ballesteros, O.; Venditto, V.; Galimberti, M.; Sartori, F.; Pucciariello, R. *J. Polym. Sci., Polym. Phys. Ed.* **1999**, *37*, 1095.

MA070757B